Ocean Engineering 36 (2009) 831–841

Contents lists available at ScienceDirect

Ocean Engineering

journal homepage: www.elsevier.com/locate/oceaneng

Interaction of flexural gravity waves with shear current in shallow water

J. Bhattacharjee [1], T. Sahoo *

Department of Ocean Engineering and Naval Architecture, Indian Institute of Technology, Kharagpur 721 302, India

ARTICLE INFO

Article history:
Received 2 October 2008
Accepted 4 May 2009
Available online 27 May 2009

Keywords:
Flexural gravity wave
Wave trapping
Wave scattering
Shear current
Jet-like current
Shallow-water approximation

ABSTRACT

In the present study, the effect of shear current on the propagation of flexural gravity waves is analyzed under the assumptions of linearized shallow-water theory. Explicit expressions for the reflection and transmission coefficients associated with flexural gravity wave scattering by a step discontinuity in both water depth and current speed are derived. Further, trapping and scattering of flexural gravity waves by a jet-like shear current with a top-hat profile are examined and certain limiting conditions for the waves to exist are derived. The effects of change in water depth, current speed, incident wavelength and the angle of incidence on the group and phase velocities as well as on the reflection and transmission characteristics are analyzed through different numerical results.

1. Introduction

Wave–current interaction is an important branch of study in the fields of coastal and offshore engineering and is a common feature in most of the marine environments. There are various reasons such as wind, tidal, thermal, and coriolis effects that generate ocean currents. As a result, wave–current interaction problems are very complex in nature and it is very difficult to analyze and derive physical insight from direct computational results. However, significant physical insight about the wave–current interaction can be obtained from simpler problems associated with long waves in shallow water even under the assumptions of linearized theory.

The influence of various types of currents on ocean wave propagation has been observed by navigators for a long time (see Isaacs, 1948). The significant effects of current are observed in the channel entrances to estuaries and bays, where ebb and flood currents can increase the wave height and the wave steepness causing severe damage to navigation. These are examples of shear current with jet-like profile, which are appreciable only over a finite region. For example, the mean discharge velocity of the Connecticut River at ebb tide can be $0.5\,\mathrm{m\,s^{-1}}$ at the mouth where the depth is of the order of 2 m. The resulting jet is roughly 100 m wide and 20 km long. At the mouth of the Ishikari River in Hokaido Japan, the depth is roughly 5 m and width 500 m; the river jet has a mean discharge velocity as high as $1\,\mathrm{m\,s^{-1}}$ extending several kilometers offshore (Mei and Lo, 1984). Another interesting phenomenon is the effect of current discontinuities in open water due to short wave breaking (see Isaacs, 1948).

Peregrine (1976) gave a comprehensive study on the interaction of water waves and currents. He discussed in detail the reasons behind the generation of currents in oceans and the effects of different kinds of currents on the propagation of ocean waves. Jonsson and Wang (1980) studied the surface gravity wave refraction by large scale currents over a gently sloping sea bed. Thomas (1981) predicted the wavelength and particle velocities under the waves by analyzing the linear wave–current interaction both experimentally and numerically. Peregrine and Jonsson (1983) presented an overview of wave–current interaction, including a comprehensive review of the literature available. Craik (1985) described the interaction between free surface gravity waves and a slowly varying, depth independent, horizontal current in water of variable depth. Hedges (1987) reviewed the progress on wave–current interaction and analyzed the effect of current on wavelength, wave periodicity, water particle kinematics, subsurface pressure, wave height, wave refraction and wave spectra. He gave an account of the situations when the complex interaction between the waves and currents was to be taken into consideration by engineers. Baddour and Song (1990) analyzed the interaction of current-free plane free surface waves of fixed frequency and a uniform wave-free current normal to the wave crest. They studied the wave height, wavelength and water depth after the interaction by using numerical methods to solve a system of nonlinear equations. Hartnack (2000) investigated the propagation of small amplitude water waves in a medium with steady uniform current and analyzed the physical phenomena of change in wavelength and wave amplitude, as well as the

* Corresponding author. Tel.: +91 3222 283792; fax: +91 3222 255303.
E-mail addresses: joydip_res@yahoo.co.in (J. Bhattacharjee), tsahoo1967@yahoo.com, tsahoo@naval.iitkgp.ernet.in (T. Sahoo).
[1] Present address: Centre for Marine Technology and Engineering, Technical University of Lisbon, Instituto Superior Tecnico, Av. Rovisco Pais, 1049-001 Lisboa, Portugal.

0029-8018/$ - see front matter © 2009 Elsevier Ltd. All rights reserved.
doi:10.1016/j.oceaneng.2009.05.008

conservation of mass, momentum and energy. On the other hand, Mei and Lo (1984) analyzed in detail the effects of jet-like currents on the propagation of shallow-water gravity waves in a homogeneous sea by analyzing the trapping and scattering of waves by a top-hat current profile. In this study, it was assumed that the current is steady and parallel and its horizontal velocity components vary only transversely. Kirby (1986) corrected the edge condition used by Mei and Lo (1984) and subsequently the results of Mei and Lo (1984). It may be noted that most of these studies are limited to wave interaction with surface gravity waves.

Flexural gravity waves are generated due to the interaction of free surface gravity waves with large floating flexible structures. This finds its application in the field of Ocean Engineering, where very large floating offshore structures are constructed for various human activities (see Chen et al., 2006; Watanabe et al., 2004), such as floating airports or floating wave energy extraction devices. These structures are assumed to be flexible in nature. On the other hand, in the cold regions of Arctic and Antarctic, vast ocean surface remains covered by a thin sheet of floating ice, which is also modeled as a floating elastic plate. There has been very little progress on the analysis of the effect of current on flexural gravity waves. Davys et al. (1985) studied the flexural gravity waves due to a steadily moving source on a floating ice sheet. Schulkes et al. (1987) investigated the effect of uniform flow beneath an ice sheet on the waves generated due to a steadily moving source. They analyzed different cases and obtained various critical aspects of the problem for both short and long waves. Recently, Squire (2007) reviewed the recent progress on the analysis of wave interaction with a floating ice sheet. Bhattacharjee and Sahoo (2007) considered the flexural gravity wave interaction with uniform currents in two dimensions in water of both finite and infinite depths. Further, Bhattacharjee and Sahoo (2008) analyzed the generation of flexural gravity waves due to initial disturbance in the presence of uniform current.

In the present study, the effect of a shear current profile on the propagation of flexural gravity waves is analyzed under the assumptions of linearized shallow-water theory. The boundary value problem is formulated in the three-dimensional Cartesian coordinate system and the floating ice sheet is modeled under the assumptions of the Euler–Bernoulli thin plate equation. The scattering of flexural gravity waves by a jet-like shear current (as shown in Fig. 1) is investigated and explicit expressions for the reflection and transmission coefficients are derived. The phenomenon of wave trapping by a jet-like shear current with a top-hat profile (as shown in Fig. 2) is analyzed and conditions for wave trapping are derived in specific cases. The energy relation involving the reflection and transmission coefficients for the case of wave scattering by a step discontinuity in both water depth and shear current speed is obtained by the application of conservation of energy flux and the continuity of the vertical deflection of the ice sheet. The group and phase velocities of flexural gravity waves in shallow water in the presence of shear current are presented in brief. Numerical results are analyzed to understand the effects of change in current speed, incident wavelength, water depth and the incident wave angle on the behavior of flexural gravity wave propagation in the presence of a shear current.

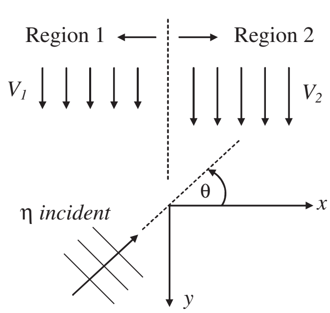

Fig. 1. Schematic diagram for the case of wave scattering by a depth/current discontinuity.

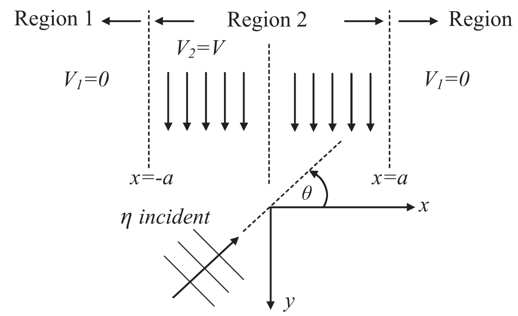

Fig. 2. Schematic diagram for the case of wave scattering and trapping by parallel depth/current discontinuities.

2. The general boundary value problem

In the present section, a linearized shallow-water equation for flexural gravity waves is formulated in the presence of a shear current. In the three-dimensional Cartesian coordinate system, the x–y plane is considered as the horizontal plane and z-axis is vertically downward positive. The fluid is assumed to be inviscid and incompressible, and the motion is irrotational. The shear current is assumed to be steady and always parallel to the y-axis. The upper surface of the fluid $-\infty<x,\ y<\infty$, $z=0$ is covered by an infinite thin elastic plate of small thickness d, which is assumed to be an ice sheet in the present study unless otherwise specified. It may be noted that in linear shallow-water theory, the vertical velocity component is a linear function of distance above the bottom. Thus, the equation of continuity in the presence of a shear current with velocity $(0, V)$ yields (see Mei and Lo, 1984 with h and V as constants)

$$h\left(\frac{\partial^2 \Phi}{\partial x^2}+\frac{\partial^2 \Phi}{\partial y^2}\right)=\frac{\partial \eta}{\partial t}+V\frac{\partial \eta}{\partial y}, \tag{1}$$

where $\eta(x,y,t)$ is the free surface displacement, $\Phi(x,y,t)$ is the velocity potential, h is the water depth, and V is a constant. On the other hand, the Euler–Bernoulli thin plate equation yields

$$\rho_i d\frac{\partial^2 \eta}{\partial t^2}=-EI\left(\frac{\partial^2 \eta}{\partial x^2}+\frac{\partial^2 \eta}{\partial y^2}\right)^2-P, \tag{2}$$

where $I=d^3/12(1-\nu^2)$, E is Young's modulus, ν is Poisson's ratio, ρ_i is the mass per unit area of the ice sheet, and P is the hydrodynamic pressure exerted on the structure. In the presence of a constant shear current $(0, V)$, the hydrodynamic pressure P is obtained from the linearized Bernoulli's equation as given by

$$P=-\rho\left(\frac{\partial \Phi}{\partial t}+V\frac{\partial \Phi}{\partial y}\right)+\rho g\eta, \tag{3}$$

where ρ is the density of water and g the acceleration due to gravity. Eliminating P and Φ from Eqs. (1) to (3) yields (similar to Bhattacharjee and Sahoo, 2007)

$$EI\left(\frac{\partial^2}{\partial x^2}+\frac{\partial^2}{\partial y^2}\right)^3\eta+\left(\rho g+\rho_i d\frac{\partial^2}{\partial t^2}\right)\left(\frac{\partial^2}{\partial x^2}+\frac{\partial^2}{\partial y^2}\right)\eta$$
$$=\frac{\rho}{h}\left(\frac{\partial}{\partial t}+V\frac{\partial}{\partial y}\right)^2\eta. \tag{4}$$

Eq. (4) is a 6th order partial differential equation in η and represents the linearized long wave equation for flexural gravity waves in the presence of a shear current under the assumptions of shallow-water theory. The above Eq. (4) can be expressed in terms of the velocity potential Φ, which is similar to Eq. (4) with η replaced by Φ. We assume that the motion is simple harmonic in time with angular frequency ω and a monochromatic wave is obliquely incident making an angle θ with the x-axis. Thus, the vertical deflection $\eta(x,y,t)$ can be expressed as $\eta(x,y,t) = \mathrm{Re}\{\zeta(x)e^{-i\beta y - i\omega t}\}$, where β is the y-component of the wave number. Hence, the long wave equation (4) will reduce to the form given by

$$EI\left(\frac{\partial^2}{\partial x^2} - \beta^2\right)^3 \zeta + (\rho g - \rho_i d\omega^2)\left(\frac{\partial^2}{\partial x^2} - \beta^2\right)\zeta = -\frac{\rho}{h}(\omega + \beta V)^2 \zeta. \tag{5}$$

Sturova (2001) used an equation describing the normal buckling of an elastic plate similar to Eq. (5), with $V = 0$. Next, the phase and group velocities of plane progressive flexural gravity waves in the presence of a shear current flow are discussed in brief.

3. Phase and group velocity

In the present section, the group and phase velocities of flexural gravity waves are analyzed to understand the effect of a shear current profile on the propagation of obliquely incident flexural gravity waves. Assuming that the motion is harmonic in time and in y-direction, the velocity potential Φ will be of the form $\Phi(x,y,t) = \mathrm{Re}\{\phi(x)e^{-i\beta y - i\omega t}\}$. Thus, the linearized long wave equation (4) can be re-expressed in terms of the velocity potential ϕ as given by

$$EI\left(\frac{\partial^2}{\partial x^2} - \beta^2\right)^3 \phi + (\rho g - \rho_i d\omega^2)\left(\frac{\partial^2}{\partial x^2} - \beta^2\right)\phi = -\frac{\rho}{h}(\omega + \beta V)^2 \phi. \tag{6}$$

A progressive wave solution for ϕ of the form $\phi(x) = e^{-i\alpha x}$ yields

$$EIk^6 + (\rho g - \rho_i d\omega^2)k^2 = \frac{\rho}{h}(\omega + \beta V)^2, \tag{7}$$

where $k^2 = \alpha^2 + \beta^2$, with $\beta = k\sin\theta$, θ is the angle made by the progressive wave with the positive x-axis. Eq. (7) is the linearized shallow-water dispersion relation for flexural gravity wave in the presence of a shear current. Analyzing the dispersion relation (7), the general expression for the group velocity c_g in the presence of a shear current is obtained as

$$c_g = nc_r - V\sin\theta, \quad n = \frac{3EIk^4 + \rho g + \rho_i d\omega kV\sin\theta - \rho_i d\omega^2}{EIk^4 + \rho g + \rho_i d\omega kV\sin\theta}, \tag{8}$$

where $c_r = c + V\sin\theta$, $c = \omega/k$ is the absolute phase velocity and c_r is the relative phase velocity. In the absence of current (i.e. $V = 0$), the above relation reduces to

$$c_g = nc_r, \quad n = \frac{3EIk^4 + \rho g - \rho_i d\omega^2}{EIk^4 + \rho g}. \tag{9}$$

On the other hand, if the thickness of the ice sheet is sufficiently small compared to the wavelength, i.e. for $\rho_i d\omega^2/\rho g \to 0$, c_g is given by Eq. (8) with

$$n = \frac{3EIk^4 + \rho g}{EIk^4 + \rho g}. \tag{10}$$

In the present study, hereafter the term involving $\rho_i d\omega^2/\rho g$ is neglected assuming the thickness of the ice sheet is sufficiently small compared to the wavelength, which is very common in the hydroelastic analysis of very large floating structures (Schulkes et al., 1987).

4. Wave scattering due to change in depth and current

In the present section, scattering of flexural gravity waves due to an abrupt change in water depth and current speed from region 1 ($x<0$) to region 2 ($x>0$) is analyzed under the assumptions of linearized shallow-water theory as shown in Fig. 1. The abrupt change in the current speed can be interpreted as a thin vortex sheets at the interface with the assumption that the flow is irrotational in the adjoining regions with uniform current. The asymptotic forms of the wave profiles in the two regions are described as

$$\zeta(x) \sim \begin{cases} e^{i\alpha_1 x} + Re^{-i\alpha_1 x}, & x<0, \\ Te^{i\alpha_2 x}, & x>0, \end{cases} \tag{11}$$

where R and T are the unknowns associated with the amplitudes of the reflected and transmitted waves, respectively, and for a given β, α_j, $j = 1,2$ is the positive real root of the dispersion relation (7) that represents the progressive wave mode. It may be noted that $-\alpha_j$ is also a solution of Eq. (7). Further, apart from the two real roots, Eq. (7) has in general four complex roots that represent the decaying (evanescent) modes. In the present study of wave scattering, only the progressive wave solutions are considered. The amplitude of the incident wave is taken as one for numerical convenience. We assume an abrupt jump in the water depth and current speed from h_1, V_1 in region 1 to h_2, V_2 in region 2. The continuity of vertical deflection of the floating ice sheet at the point of discontinuity at $x = 0$ yields

$$1 + R = T. \tag{12}$$

On the other hand, conservation of energy flux yields

$$\frac{\mathscr{E}}{\sigma}(c_g + V\sin\theta) = \text{constant}, \tag{13}$$

where $\sigma = \omega + kV\sin\theta$ is the relative wave frequency, $\mathscr{E} = H^2(EIk^4 + \rho g)/8$ is the total wave energy for flexural gravity waves with H as the wave height (i.e. twice the wave amplitude). It may be noted that the total energy in case of flexural gravity waves is the combination of kinetic, potential and surface energy. The surface energy is generated here due to the presence of the floating ice sheet. Substituting σ and $\mathscr{E}$ in (13), the energy relation involving R and T is obtained as

$$1 - R^2 = \gamma T^2, \quad \gamma = \frac{(EIk_2^4 + \rho g)(c_{g2} + V_2\sin\theta)\sigma_1}{(EIk_1^4 + \rho g)(c_{g1} + V_1\sin\theta)\sigma_2}, \tag{14}$$

where the subscripts 1 and 2 denote the values of the parameters in the respective regions. Solving the two Eqs. (12) and (14), the reflection and transmission coefficients R and T are obtained as

$$R = \frac{1-\gamma}{1+\gamma}, \quad T = \frac{2}{1+\gamma}. \tag{15}$$

5. Wave trapping

In this section, the conditions for existence of trapped modes of flexural gravity waves in the presence of a jet-like shear current with a top-hat profile (Mei and Lo, 1984) are studied. The entire fluid domain is divided into two regions, namely region 1 ($|x|>a$) and region 2 ($|x|<a$) as shown in Fig. 2. It is assumed that the current is in the positive y-direction and the distribution is

of the form

$$V(x)=\begin{cases} V=\text{constant}>0, & |x|<a,\\ 0, & |x|>a. \end{cases} \tag{16}$$

Hence, the linearized shallow-water equation (5) for flexural gravity wave yields

$$\begin{aligned} &\left\{D\frac{\partial^6}{\partial x^6}-3\beta^2D\frac{\partial^4}{\partial x^4}+\left(3\beta^4D+\frac{1}{\beta^2}\right)\frac{\partial^2}{\partial x^2}+K^2-G^2\right\}\zeta=0, \quad |x|>a,\\ &\left\{D\frac{\partial^6}{\partial x^6}-3\beta^2D\frac{\partial^4}{\partial x^4}+\left(3\beta^4D+\frac{1}{\beta^2}\right)\frac{\partial^2}{\partial x^2}+(K+F)^2-G^2\right\}\zeta=0,\\ &\quad |x|<a, \end{aligned} \tag{17}$$

where $D=EI/\rho g\beta^2$, $K=\omega/\beta\sqrt{gh}$, $F^2=V^2/gh$ and $G=\sqrt{1+D\beta^6}$. Thus, varying the physical parameters ω and β, different types of physical problems of flexural gravity waves can be modeled. The waves will be trapped if there exists, at a given frequency, a propagating wave-like solution in the region $|x|<a$, accompanied by a solution that decays exponentially toward the far field in the region $|x|>a$. Hence, in the case of trapped modes inside the top-hat current profile, the vertical deflection $\zeta(x)$ is given by

$$\zeta(x)\sim\begin{cases} Ae^{\alpha_1(x+a)}, & x<-a,\\ Be^{i\alpha_2 x}+Ce^{-i\alpha_2 x}, & |x|<a,\\ De^{-\alpha_1(x-a)}, & x>a, \end{cases} \tag{18}$$

where A, B, C and D are the unknown constants associated with the wave amplitudes. From Eqs. (17) and (18), it is easily derived that the wave number α_1 satisfies the equation

$$D\alpha_1^6-3\beta^2D\alpha_1^4+\left(3\beta^4D+\frac{1}{\beta^2}\right)\alpha_1^2+K^2-G^2=0, \tag{19}$$

whereas α_2 satisfies

$$D\alpha_2^6+3\beta^2D\alpha_2^4+\left(3\beta^4D+\frac{1}{\beta^2}\right)\alpha_2^2-\{(K+F)^2-G^2\}=0. \tag{20}$$

Eq. (19) will have a real root if

$$K<G. \tag{21}$$

On the other hand, Eq. (20) will have a real root if

$$G-F<K. \tag{22}$$

The inequalities in Eqs. (21) and (22) provide the conditions for flexural gravity wave trapping in a region having a jet-like current with top-hat profile. The vertical deflection ζ of the ice sheet is assumed to be continuous at the interface $x=\pm a$, which yields

$$\zeta|_{x=\pm a^-}=\zeta|_{x=\pm a^+}. \tag{23}$$

Eq. (23) provides two equations with four unknowns A, B, C and D. Thus, we need two more conditions, which can be derived from the shallow-water equation (5). The linearized shallow-water equation for flexural gravity waves can be written in the form

$$\left[\delta_j\frac{\partial^6}{\partial x^6}-3\beta^2\delta_j\frac{\partial^4}{\partial x^4}+(3\beta^4\delta_j+\mu_j)\frac{\partial^2}{\partial x^2}+\{1-(\beta^4\delta_j+\mu_j)\beta^2\}\right]\zeta=0,\quad j=1,2, \tag{24}$$

where $\mu_1=gh/\omega^2$, $\mu_2=gh/(\omega+\beta V)^2$, $\delta_1=EIh/\rho\omega^2$ and $\delta_2=EIh/\rho(\omega+\beta V)^2$. Integrating Eq. (24) between $x=\pm a-\varepsilon$ and $x=\pm a+\varepsilon$ where $\varepsilon\to 0$ and assuming the continuity of shear force, bending moment, slope of deflection and the deflection of the ice sheet at $x=\pm a$, it can be derived that

$$\delta_2\left.\frac{\partial^5\zeta}{\partial x^5}\right|_{x=a^-}=\delta_1\left.\frac{\partial^5\zeta}{\partial x^5}\right|_{x=a^+},\quad \delta_1\left.\frac{\partial^5\zeta}{\partial x^5}\right|_{x=-a^-}=\delta_2\left.\frac{\partial^5\zeta}{\partial x^5}\right|_{x=-a^+}. \tag{25}$$

Eq. (25) provides a higher order edge condition for flexural gravity waves and accounts for the higher order term present in the shallow-water equation due to the floating ice sheet.

Using the continuity of the deflection of the ice sheet at $x=\pm a$ as in Eq. (23) along with the two edge conditions in Eq. (25) at $x=\pm a$, from Eq. (18), a homogeneous system of four equations is obtained in terms of A, B, C and D. For a non-trivial solution of the system of homogeneous equations, an eigenvalue condition is obtained as given by

$$\tan 2\alpha_2 a=\tan 2\delta, \tag{26}$$

with $\delta=\tan^{-1}\{\delta_1\alpha_1^5\}/\{\delta_2\alpha_2^5\}$. From Eq. (26), it is easily derived that

$$\delta=\frac{n\pi}{2}+\alpha_2 a \quad \text{for } n=0,1,2,\ldots. \tag{27}$$

Thus, from Eqs. (26) and (27), the condition for trapped modes is obtained as

$$\frac{\delta_1\alpha_1^5}{\delta_2\alpha_2^5}=\begin{cases} \tan\alpha_2 a & \text{in case } n \text{ is even},\\ -\cot\alpha_2 a & \text{in case } n \text{ is odd}. \end{cases} \tag{28}$$

6. Wave scattering by top-hat current

In this section, scattering of flexural gravity waves by a top-hat current profile is analyzed under the shallow-water approximation. The form of the jet-like shear current with a top-hat profile is the same as described in Eq. (16) and shown in Fig. 2. In the case of wave scattering, it is required to have propagating wave-like solutions everywhere in the domain of consideration. Eq. (17) will have a wave-like solution of the form

$$\zeta(x)\sim\begin{cases} e^{i\alpha_1(x+a)}+Re^{-i\alpha_1(x+a)}, & x<-a,\\ Ae^{i\alpha_2 x}+Be^{-i\alpha_2 x}, & |x|<a,\\ Te^{i\alpha_1(x-a)}, & x>a, \end{cases} \tag{29}$$

provided

$$\begin{aligned} &K^2>G^2 && \text{in region 1},\\ &(K+F)^2>G^2 && \text{in region 2}. \end{aligned} \tag{30}$$

In the present study, the length of the intermediate region is assumed to be large in comparison to the incident wavelength. Thus, the decaying modes do not affect the wave motion inside the shear current region and only progressive waves are considered. It may be further observed that for $\beta>0$, the incident angle θ lies in $0<\theta<90^\circ$, where $\theta=\sin^{-1}(\beta/k)$, and hence the waves will be propagating against the current. On the other hand, for $\beta<0$, θ lies in $-90^\circ<\theta<0$ and the waves will be propagating along with the current provided $K<-G$. Further, for $\beta<0$ the condition for region 2 in Eq. (30) is modified to the form given by

$$K<-G-F. \tag{31}$$

The regions for wave trapping and scattering due to a top-hat current are shown in Fig. 3 for clarity. Next, the flexural gravity wave scattering by a top-hat current will be analyzed by determining the unknown constants R and T. Using the continuity of the deflection of the ice sheet at $x=\pm a$ as in Eq. (23) along with the edge conditions at $x=\pm a$ as in Eq. (25), the constants R and T associated with the reflected and transmitted wave amplitudes are obtained as

$$\begin{aligned} R&=\frac{-(1-b^2)[e^{-2i\alpha_2 a}-e^{2i\alpha_2 a}]}{(1+b)^2e^{-2i\alpha_2 a}-(1-b)^2e^{2i\alpha_2 a}},\\ T&=\frac{4b}{(1+b)^2e^{-2i\alpha_2 a}-(1-b)^2e^{2i\alpha_2 a}}, \end{aligned} \tag{32}$$

where $b=\alpha_1^5(\omega+\beta V)^2/\alpha_2^5\omega^2$. The explicit expressions for the square of the reflection and transmission coefficients $|R|$ and $|T|$

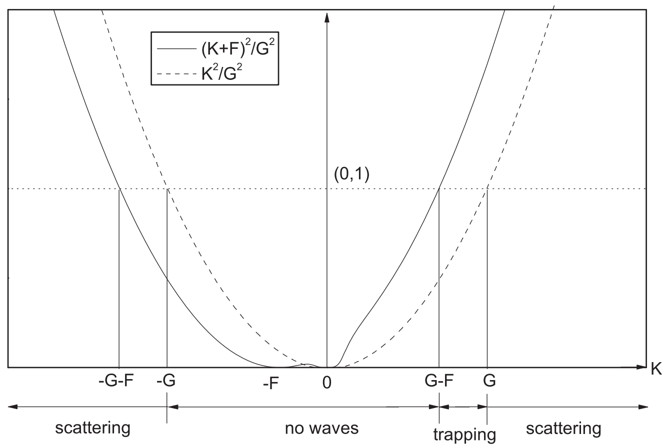

Fig. 3. Regions of flexural gravity wave trapping and scattering.

are given by

$$|R|^2 = \frac{(1-b^2)^2 \sin^2(2\alpha_2 a)}{4b^2 + (1-b^2)^2 \sin^2(2\alpha_2 a)},$$
$$|T|^2 = \frac{4b^2}{4b^2 + (1-b^2)^2 \sin^2(2\alpha_2 a)}. \tag{33}$$

It is evident from the expressions in Eq. (33) that $|R|$ exhibits a periodic behavior with the scatter parameter $\alpha_2 a$, and is equal to zero when $b=1$ or when $2\alpha_2 a = n\pi$. Further, it can be observed from Eq. (33) that the reflection and transmission coefficients $|R|$ and $|T|$ satisfy

$$|R|^2 + |T|^2 = 1. \tag{34}$$

The above relation can also be derived from the conservation of energy flux and is termed the energy relation. This energy relation provides a numerical check for the computed results for reflection and transmission coefficients.

7. Numerical results and discussion

In this section, simple numerical computations are performed to study the effects of jet-like current, water depth, thickness of the ice sheet and rigidity of the ice sheet on the propagation of flexural gravity waves. The results and discussions are based on the evaluation of reflection coefficient, transmission coefficient, phase velocity and group velocity. The numerical values of the physical parameters which are fixed throughout the computation are $\rho = 1025\,\mathrm{kg\,m^{-3}}$, $\rho_i = 922.5\,\mathrm{kg\,m^{-3}}$, $\nu = 0.3$ and $g = 9.8\,\mathrm{m\,s^{-2}}$.

7.1. Wave number, phase and group velocity

In Fig. 4, the variation of flexural gravity wave number k versus wave frequency ω is plotted for various values of water depth h in the presence of a jet-like current. It is observed that the wave number increases with increasing wave frequency for all water depths. Further, the wave number k decreases with increase in the values of water depth h, which is evident also from the shallow-water dispersion relation as in Eq. (7). This in turn shows that the phase velocity c increases with an increase in the water depth h.

Fig. 5 shows the variation of flexural gravity wave number k versus wave frequency ω for various values of a jet-like current speed V. It is observed that the wave number k increases with increasing wave frequency ω for all values of current speed V. Further, it may be noted that k increases with increasing current speed for $V>0$. However, k decreases for opposing current, i.e., for $V<0$. These observations suggest that the phase velocity c decreases with an increase in positive current speed.

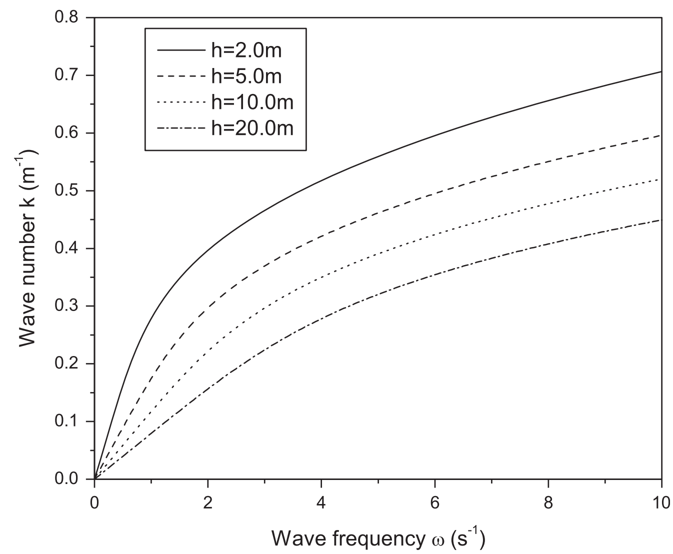

Fig. 4. Wave number k versus wave frequency ω for various values of water depth h with $\theta = 45^\circ$, $d = 0.1\,\mathrm{m}$, $E = 5\,\mathrm{GPa}$ and $V = 2\,\mathrm{m\,s^{-1}}$.

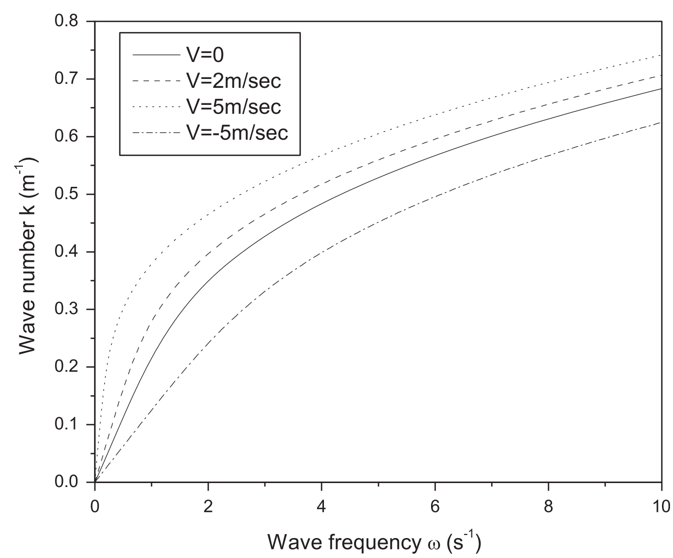

Fig. 5. Wave number k versus wave frequency ω for various values of current speed V with $\theta = 45^\circ$, $d = 0.1\,\mathrm{m}$, $E = 5\,\mathrm{GPa}$ and $h = 2\,\mathrm{m}$.

In Fig. 6, the variation of flexural gravity wave number k versus wave frequency ω is plotted for various values of the plate thickness d in the presence of a jet-like current. As in Figs. 4 and 5, in this case also, the wave number k increases with wave frequency ω for all values of plate thickness d. On the other hand, the wave number k decreases and hence the phase velocity c increases with increase in the values of plate thickness d. Further, the variation in the values of the wave number k with increasing wave frequency ω is comparatively small for plate thickness $d \geq 0.5\,\mathrm{m}$.

In Figs. 7(a) and (b), respectively, phase and group velocities c and c_g versus wave number k are plotted for various values of water depth h for shallow-water flexural gravity waves in the presence of a jet-like current. It is observed that as h increases, c also increases steadily. On the other hand, up to a particular value of the wave number, c_g increases with increasing h and then starts decreasing. Finally, c_g again increases with increasing h. It is further observed that both c and c_g increase with increasing wave number. In addition, $c_g > c$, i.e. for flexural gravity waves the wave energy moves faster than the individual waves.

In Figs. 8(a) and (b), respectively, c and c_g versus k are plotted for different values of the current speed V. It is observed that as V increases, the phase velocity c decreases. This is due to the fact that in case of positive incident angle, the waves are propagating opposite to the current direction for $V>0$ whereas waves propagate along with the current when $V<0$. The group velocity c_g decreases with increase in V up to a certain wave number, and beyond that c_g starts increasing with increase in V.

Figs. 9(a) and (b), respectively, show the variation of c and c_g versus k for various values of incident angle θ. It may be noted that c decreases with increase in θ and the decrease is more evident for smaller values of k. On the other hand, c_g decreases with increase in θ for smaller values of k and as k increases, c_g increases with an increase in θ. Further, it is observed that $c_g > c$ for a particular wave number which indicates that the propagation speed of an individual wave is smaller than the rate at which the wave energy propagates.

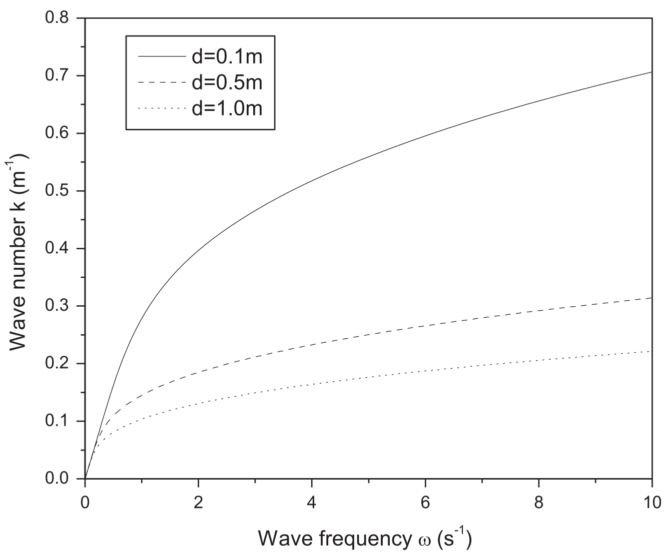

Fig. 6. Wave number k versus wave frequency ω for various values of plate thickness d with $\theta = 45^\circ$, $E = 5\,\text{GPa}$, $V = 2\,\text{m}\,\text{s}^{-1}$ and $h = 2\,\text{m}$.

7.2. Wave scattering due to change in depth and current

In this subsection, the flexural gravity wave scattering due to an abrupt change in the water depth and current speed is analyzed by studying the reflection coefficient characteristics.

Fig. 10 shows the variation of the reflection coefficient $|R|$ versus wave frequency ω for various values of ice thickness d. The reflection coefficient $|R|$ initially increases with increasing ω and attains a maximum. Then, it starts decreasing with ω. It is further observed that the maximum values of $|R|$ are attained at lower frequencies as d increases. In addition, after attaining the maximum, the rate of decrease in $|R|$ reduces as d decreases.

In Fig. 11, $|R|$ is plotted versus ω for different values of the water depth h_1 with $h_2 = 2\,\text{m}$ and $V_1 = V_2 = 5\,\text{m}\,\text{s}^{-1}$. The figure shows that, at very low frequencies, initially $|R|$ decreases with increasing ω and attains a minimum value. After attaining the minimum, $|R|$ rises sharply to attain a maximum and then decreases slowly with frequency. It may also be noted that as h_1 decreases, the minimum values of $|R|$ are attained at a lower wave frequency. Further, $|R|$ decreases with decrease in the water depth h_1.

Fig. 12 shows the variation of $|R|$ versus ω for various values of θ. It is observed that for smaller values of θ, $|R|$ attains zero minimums, whilst $|R|$ attains maximums for higher values of θ. Further, the wave reflection increases with increase in the angle of incidence.

Fig. 13 shows the variation of $|R|$ versus ω for various values of current speed V_2 with $V_1 = 2\,\text{m}\,\text{s}^{-1}$ and $h_1 = h_2 = 10\,\text{m}$. It is observed that $|R|$ increases with increase in ω and attains a maximum. After attaining the maximum, $|R|$ starts decreasing. Further, $|R|$ increases with increase in positive current speed. A similar observation is made when the magnitude of the negative current speed increases.

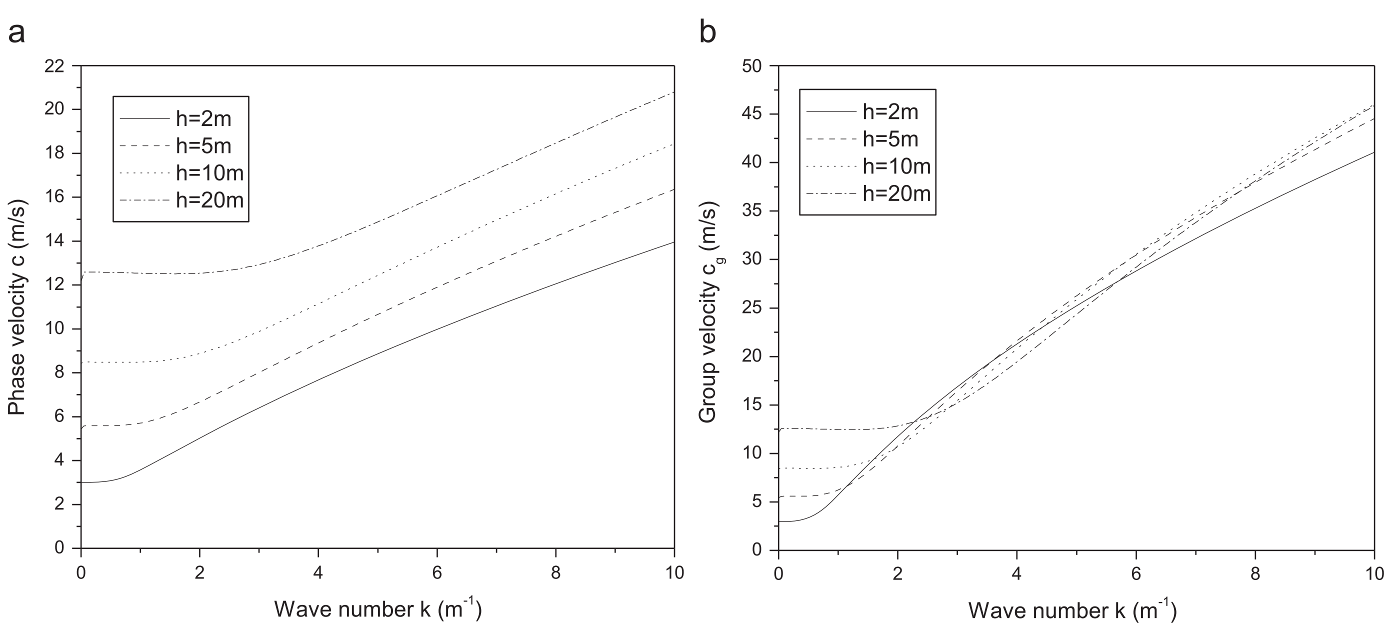

Fig. 7. (a) Phase velocity c and (b) group velocity c_g versus wave number k for various values of water depth h with $\theta = 45^\circ$, $d = 0.1\,\text{m}$, $E = 5\,\text{GPa}$ and $V = 2\,\text{m}\,\text{s}^{-1}$.

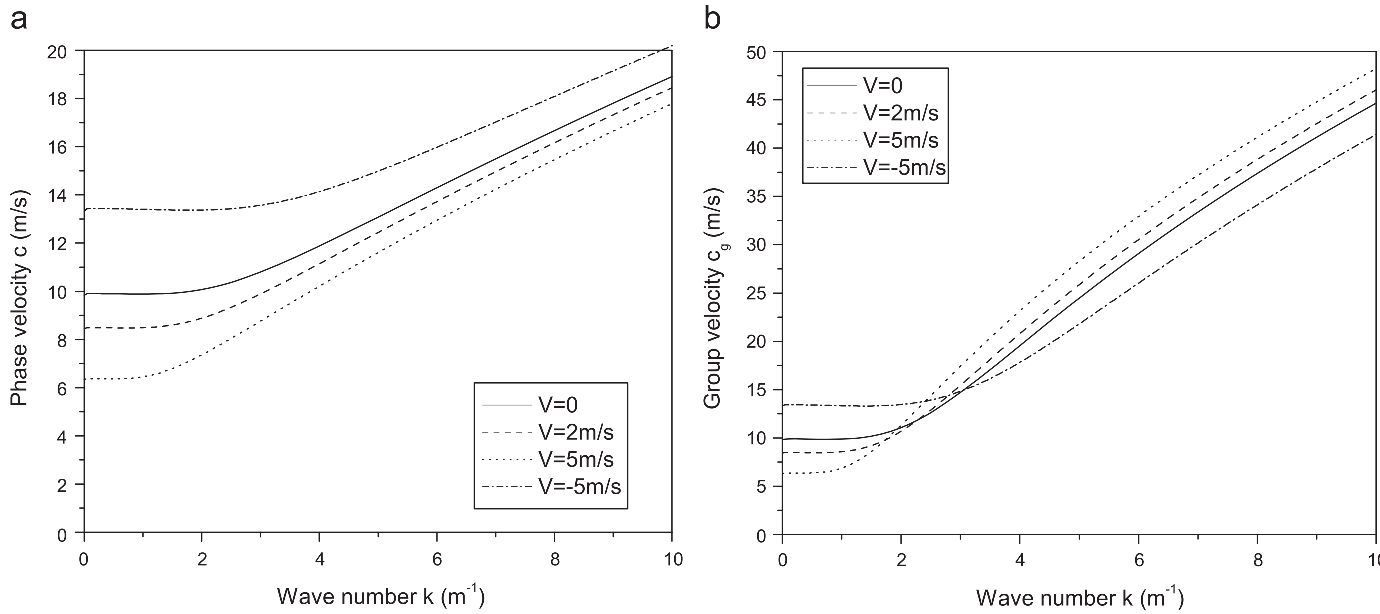

Fig. 8. (a) Phase velocity c and (b) group velocity c_g versus wave number k for various values of current speed V with $\theta = 45^\circ$, $d = 0.1\,\mathrm{m}$, $E = 5\,\mathrm{GPa}$ and $h = 10\,\mathrm{m}$.

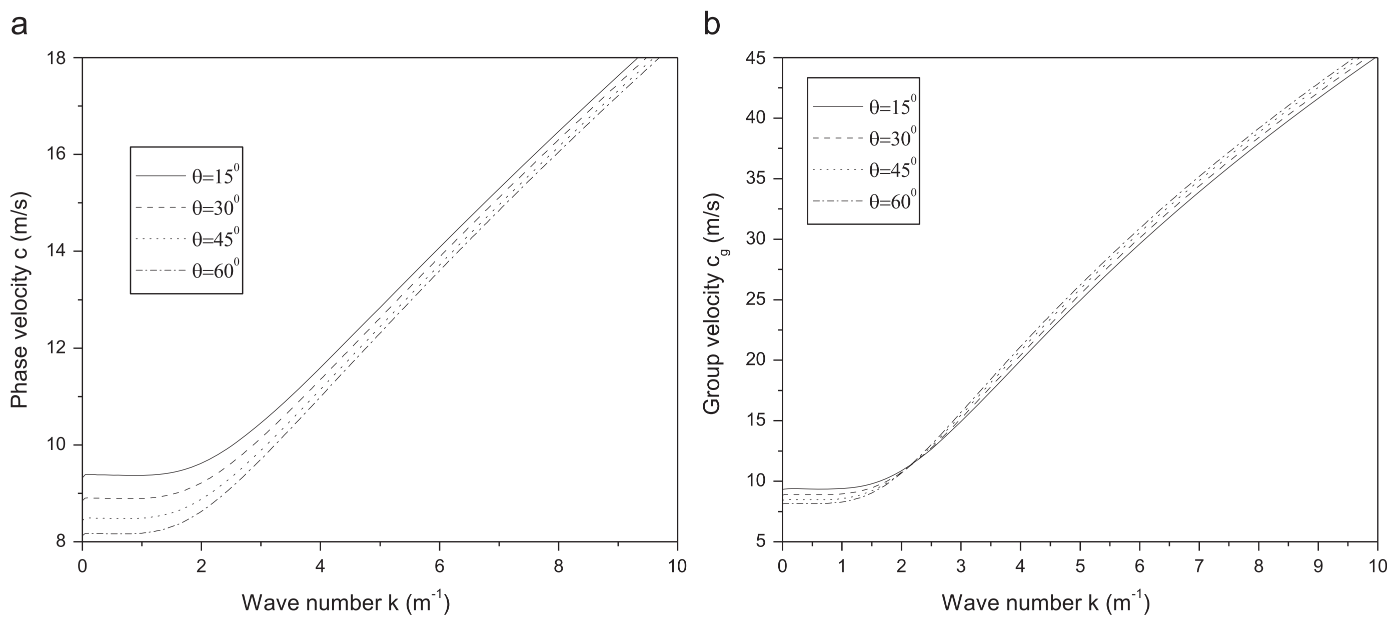

Fig. 9. (a) Phase velocity c and (b) group velocity c_g versus wave number k for various values of incident angle θ with $d = 0.1\,\mathrm{m}$, $E = 5\,\mathrm{GPa}$, $V = 2\,\mathrm{m\,s^{-1}}$ and $h = 10\,\mathrm{m}$.

7.3. *Wave scattering by top-hat current*

In this subsection, the scattering of flexural gravity waves by a top-hat current profile is analyzed by studying the reflection coefficient characteristics. Fig. 14 shows $|R|$ versus ka for various values of the water depth h. It is observed that $|R|$ increases with decrease in h for a particular current speed and incident angle. Further, $|R|$ exhibits a periodic behavior with ka with the magnitude of the peak values decreasing as ka increases, which is evident also from the explicit expressions of $|R|$ in Eq. (33). In addition, the period of the oscillations in $|R|$ is increasing with increase in h. This is due to the fact that the period of the oscillations in $|R|$ is proportional to the wave number component α_2, which is in turn dependent on the water depth h.

Figs. 15(a)–(c) show the variation of $|R|$ versus ka for various values of $\theta > 0^\circ$ for three different cases of $F = 0.1$, 0.3 and 0.5, respectively. It may be observed that the minimums attained by $|R|$ are almost zero for $F = 0.1$, but $|R|$ never reaches a zero minimum in the other two cases of $F = 0.3$ and 0.5. This may be due to the difference in the phase of the incident and reflected waves when the wave interacts with the current. As the current speed increases, the period of the oscillations in $|R|$ with respect to ka decreases. This is evident from Eq. (33), which shows that the period of the oscillations in $|R|$ is proportional to α_2, and in turn dependent on the current speed V. The above fact demonstrates the dominating role of the jet-like current on the propagation of flexural gravity waves. Further, it is observed that in all the three cases, as θ increases, $|R|$ increases. In addition, as $\theta > 0^\circ$ implies

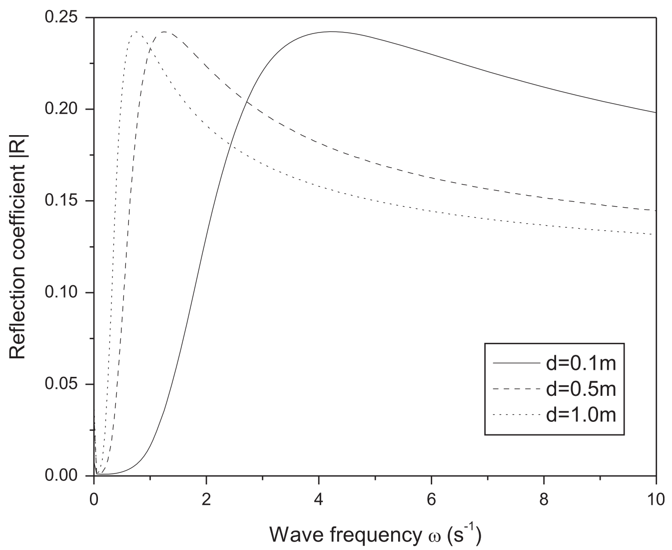

Fig. 10. Reflection coefficient $|R|$ versus wave frequency ω for various values of plate thickness d with $\theta = 30^\circ$, $E = 5\,\text{GPa}$, $h_1 = 15\,\text{m}$, $h_2 = 10\,\text{m}$, $V_1 = 2\,\text{m}\,\text{s}^{-1}$, $V_2 = 5\,\text{m}\,\text{s}^{-1}$.

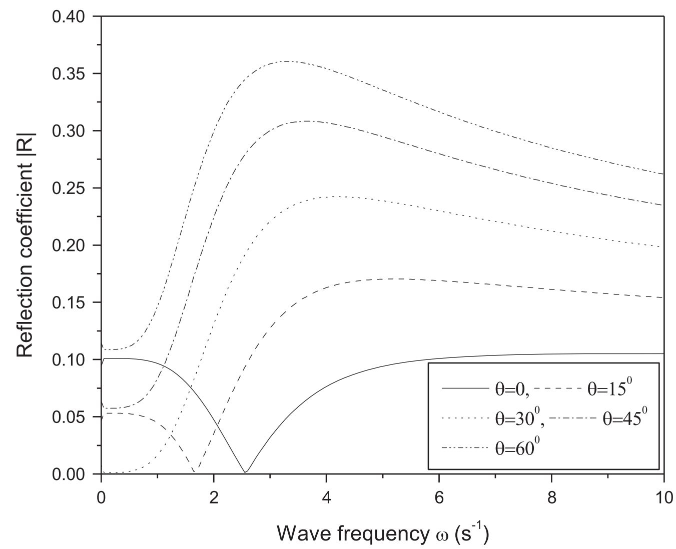

Fig. 12. Reflection coefficient $|R|$ versus wave frequency ω for various values of angle of incidence θ with $h_1 = 15\,\text{m}$, $h_2 = 10\,\text{m}$, $V_1 = 2\,\text{m}\,\text{s}^{-1}$, $V_2 = 5\,\text{m}\,\text{s}^{-1}$, $d = 0.1\,\text{m}$, $E = 5\,\text{GPa}$.

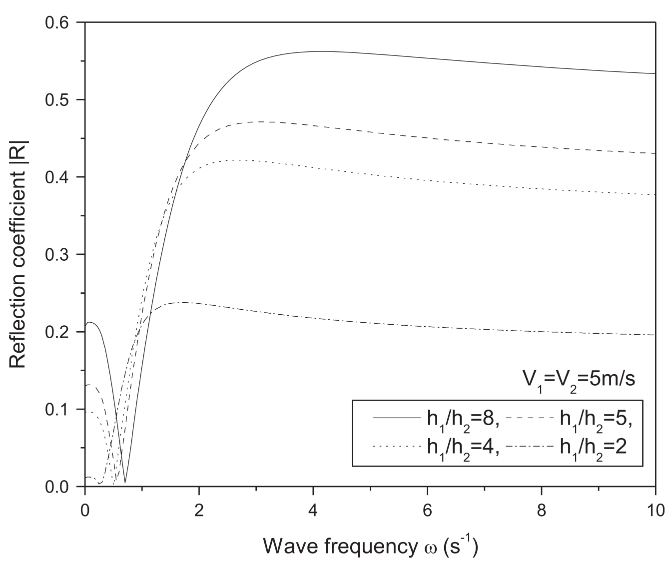

Fig. 11. Reflection coefficient $|R|$ versus wave frequency ω for various values of water depth h_1/h_2 with $\theta = 30^\circ$, $d = 0.1\,\text{m}$, $E = 5\,\text{GPa}$.

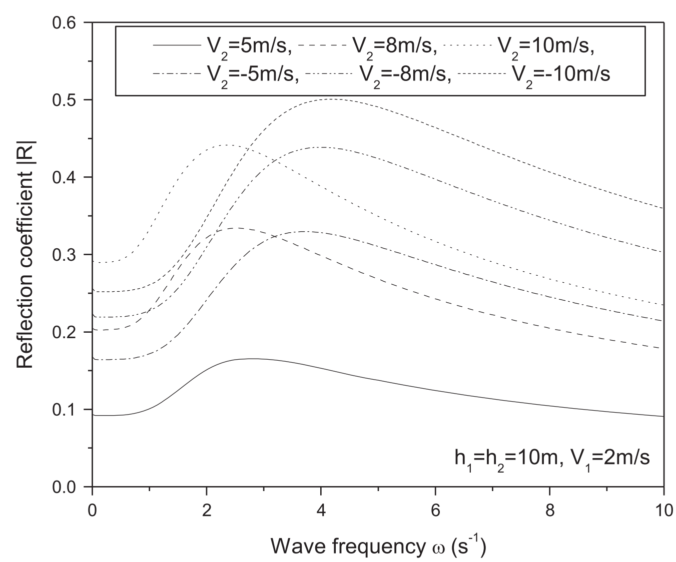

Fig. 13. Reflection coefficient $|R|$ versus wave frequency ω for various values of current speed V_2 with $\theta = 30^\circ$, $d = 0.1\,\text{m}$, $E = 5\,\text{GPa}$.

that the waves are propagating against the current, it is evident from the three figures that a stronger current causes more reflection and subsequently less transmission of wave energy. As θ approaches 90°, $|T| \to 0$ and $|R| \to 1$. In addition for $\theta = 90^\circ$, complete reflection of the plane progressive wave occurs. This is due to the fact that the wave and current headings are opposing each other and the current will disrupt the propagation of the plane progressive wave. On the other hand, as θ approaches 0°, the waves become nearly perpendicular to the direction of current. Thus, $|R|$ is verysmall and almost all the wave energy is transmitted.

Figs. 16(a)–(c) show $|R|$ versus ka for various values of $\theta < 0^\circ$ for three different cases of $F = 0.1$, 0.3 and 0.5, respectively. The pattern of $|R|$ is similar to the observations made in Fig. 15 except that the period of oscillations of $|R|$ with ka is comparatively larger in Fig. 16. However, for a particular current speed, there exists a limiting value of θ for which $|R|$ becomes almost 1. This is due to the fact that beyond this value of θ, progressive wave propagation is not possible. Hence, beyond this limiting angle, no progressive waves exist and this angle may be referred as a critical angle. A similar conclusion has been made in Section 6 for $K < -G - F$.

In Fig. 17, $|R|$ versus ka is plotted for various values of d. It is observed that as d increases, $|R|$ decreases significantly for a particular current speed and incident angle. Further, as ka increases, the magnitude of the maxima attained by $|R|$ decreases. In case of $d = 1\,\text{m}$, the reflection curve dies down to almost zero beyond $ka = 7$. This may be attributed to the fact that the period of oscillations in $|R|$ and the quantity b are dependent on the ice thickness d.

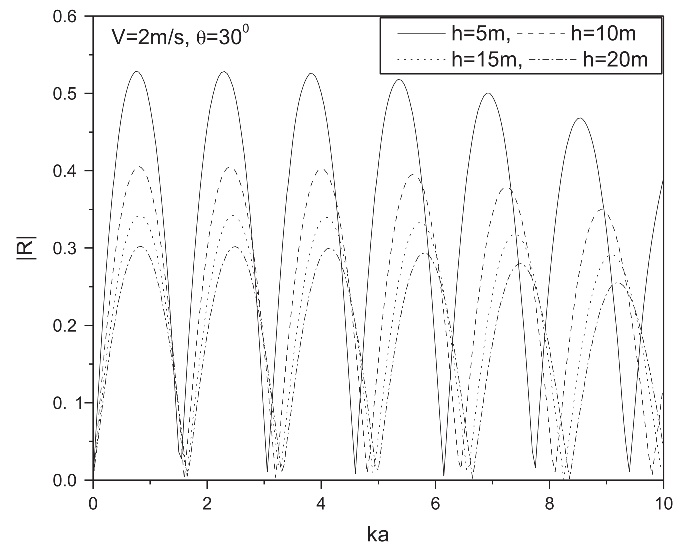

Fig. 14. Reflection coefficient $|R|$ versus ka for various values of water depth h with $\theta = 30^{\circ}$, $d = 0.1$ m, $E = 5$ GPa and $a = 50$ m.

8. Conclusion

The interaction of shear current with flexural gravity waves is analyzed under the assumptions of linearized shallow-water theory. The effect of shear current on phase and group velocities associated with a flexural gravity wave is studied. In the case of oblique waves, beyond certain values of the wave number, the group velocity is larger than the phase velocity. Explicit expressions for the reflection and transmission coefficients due to wave scattering by a step discontinuity in both water depth and shear current speed are obtained by applying conservation of energy flux and enforcing the continuity of the vertical deflection of the ice sheet. Certain extreme values in the reflection characteristics are observed in different cases. Further, trapping and scattering of flexural gravity waves by a jet-like shear current with a top-hat profile are investigated. The trapping and scattering zones for flexural gravity waves in the presence of a jet-like current are obtained theoretically and presented graphically. Limiting conditions in the case of trapping and scattering of flexural gravity waves are derived. Numerical results show multiple local extremes in the case of wave scattering by a top-hat current

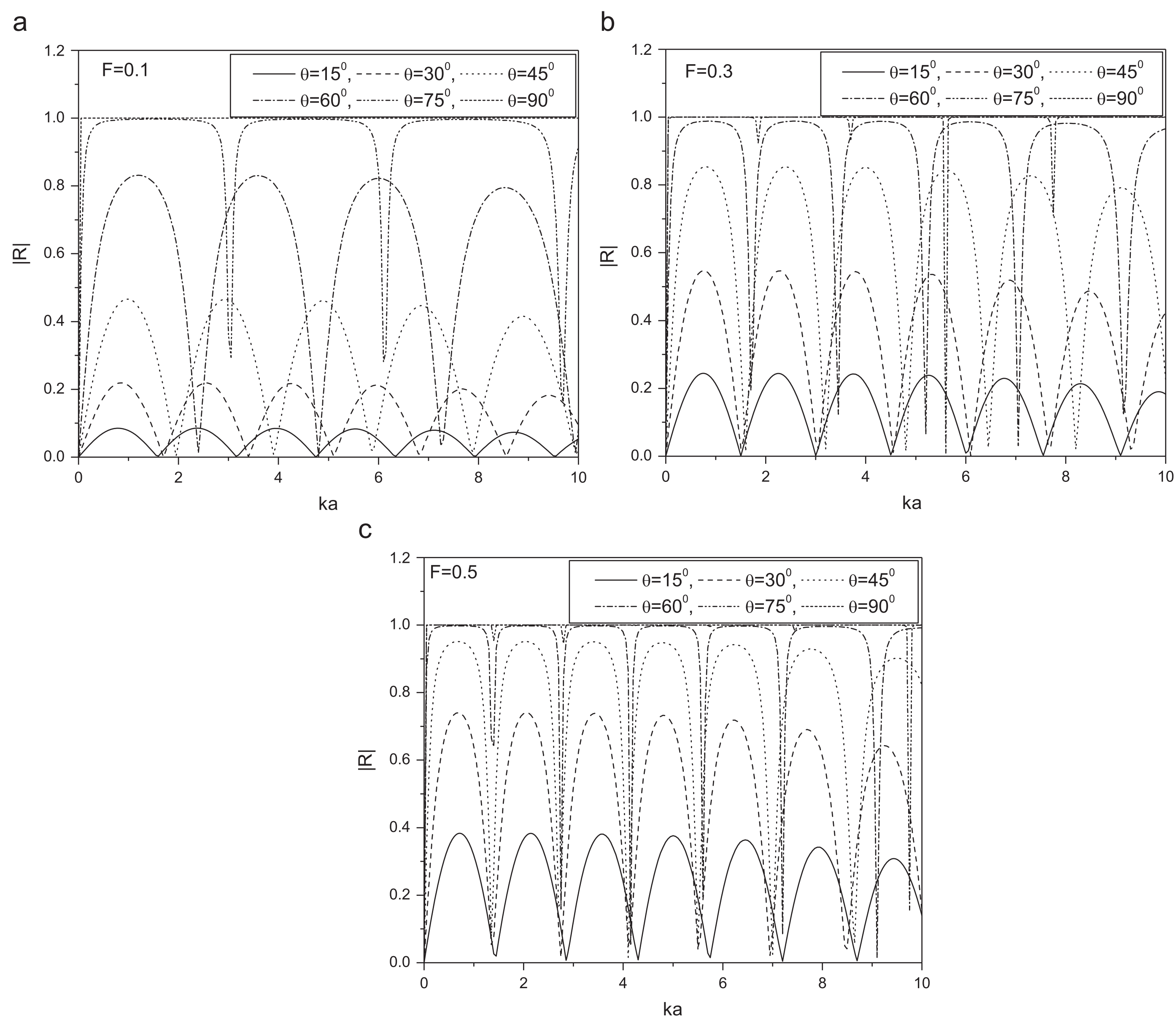

Fig. 15. Reflection coefficient $|R|$ versus ka for various values of angle of incidence $\theta > 0^{\circ}$ with $h = 10$ m, $d = 0.1$ m, $E = 5$ GPa, $a = 50$ m and (a) $F = 0.1$, (b) $F = 0.3$, (c) $F = 0.5$.

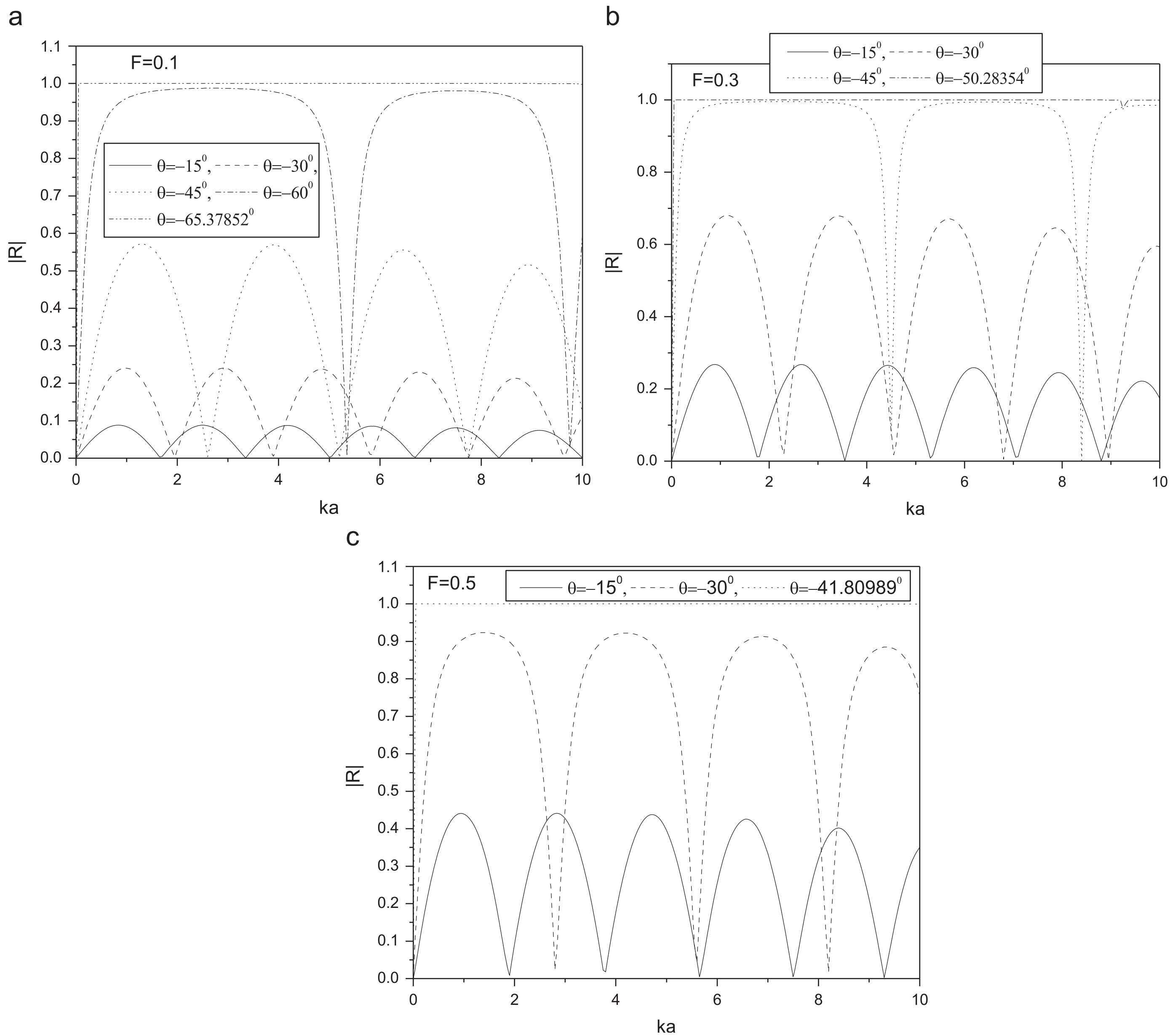

Fig. 16. Reflection coefficient $|R|$ versus ka for various values of angle of incidence $\theta<0^{\circ}$ with $h=10\,\text{m}$, $d=0.1\,\text{m}$, $E=5\,\text{GPa}$, $a=50\,\text{m}$ and (a) $F=0.1$, (b) $F=0.3$, (c) $F=0.5$.

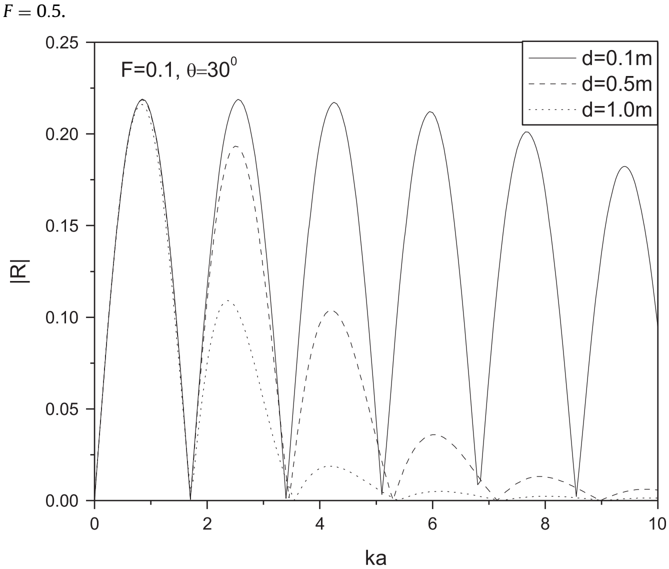

Fig. 17. Reflection coefficient $|R|$ versus ka for various values of plate thickness d with $\theta=30^{\circ}$, $h=10\,\text{m}$, $E=5\,\text{GPa}$ and $a=50\,\text{m}$.

profile. The results will be of significant importance to the study of wave–current interaction in the fields of Coastal, Offshore and Arctic Engineering.

Acknowledgment

J.B. acknowledges the financial support received from NBHM, DAE, Govt. of India, in terms of Post Doctoral Fellowship.

References

Baddour, R.E., Song, S., 1990. On the interaction between waves and currents. Ocean Engineering 17 (1/2), 1–21.

Bhattacharjee, J., Sahoo, T., 2007. Interaction of current and flexural gravity waves. Ocean Engineering 34 (11–12), 1505–1515.

Bhattacharjee, J., Sahoo, T., 2008. Generation of flexural gravity waves in the presence of uniform current. Journal of Marine Science and Technology 13, 138–146.

Chen, X., Wu, Y., Cui, W., Jensen, J.J., 2006. Review of hydroelasticity theories for global response of marine structures. Ocean Engineering 33, 439–457.

Craik, A.D.D., 1985. Wave Interactions and Fluid Flows. Cambridge University Press, Cambridge.
Davys, J.W., Hosking, R.J., Sneyd, A.D., 1985. Waves due to a steadily moving source on a floating ice plate. Journal of Fluid Mechanics 158, 269–287.
Hartnack, J.N., 2000. Short gravity waves on steady non-uniform currents obtained through up-/downwelling. Ocean Engineering 27, 417–444.
Hedges, T.S., 1987. Combinations of waves and currents: an introduction. Proceedings of the Institution of Civil Engineers. Part 1 82, 567–585.
Isaacs, J.D., 1948. Discussion of ''Refraction of surface waves by currents'' by Johnson, J.W. Transactions of the American Geophysical Union 29, 739–742.
Jonsson, I.G., Wang, J.D., 1980. Current-depth refraction of water waves. Ocean Engineering 7, 153–171.
Kirby, J.T., 1986. Comments on ''The effects of a jet-like current on gravity waves in shallow water''. Journal of Physical Oceanography 16, 395–397.
Mei, C.C., Lo, E., 1984. The effects of a jet-like current on gravity waves in shallow water. Journal of Physical Oceanography 14, 471–477.
Peregrine, D.H., 1976. Interaction of water waves and currents. Advances in Applied Mechanics 16, 9–117.
Peregrine, D.H., Jonsson, I.G., 1983. Interaction of waves and currents. Miscellaneous Report 83-6, U.S. Army Coastal Engineering Research Center, 88pp.
Schulkes, R.M.S.M., Hosking, R.J., Sneyd, A.D., 1987. Waves due to a steadily moving source on a floating ice plate. Part 2. Journal of Fluid Mechanics 180, 297–318.
Squire, V.A., 2007. Of ocean waves and sea-ice revisited. Cold Regions Science and Technology 49, 110–133.
Sturova, I.V., 2001. The diffraction of surface waves by an elastic platform floating on shallow water. Journal of Applied Mathematics and Mechanics 65 (1), 109–117.
Thomas, G.P., 1981. Wave–current interactions: an experimental and numerical study. Part 1. Linear waves. Journal of Fluid Mechanics 110, 457–474.
Watanabe, E., Utsunomiya, T., Wang, C.M., 2004. Hydroelastic analysis of pontoon-type VLFS: a literature survey. Engineering Structures 26, 245–256.